Accepted Manuscript

Freeze-thaw fracturing in building granites

D.M. Freire-Lista, R. Fort, M.J. Varas-Muriel

PII: S0165-232X(15)00009-9
DOI: doi: 10.1016/j.coldregions.2015.01.008
Reference: COLTEC 2069

To appear in: *Cold Regions Science and Technology*

Received date: 30 May 2014
Revised date: 20 January 2015
Accepted date: 22 January 2015

Please cite this article as: Freire-Lista, D.M., Fort, R., Varas-Muriel, M.J., Freeze-thaw fracturing in building granites, *Cold Regions Science and Technology* (2015), doi: 10.1016/j.coldregions.2015.01.008

FREEZE-THAW FRACTURING IN BUILDING GRANITES

Freire-Lista, D. M.[1,2]*, Fort, R.[1,2], Varas-Muriel, M. J.[1,3]

(1) Instituto de Geociencias IGEO (CSIC, UCM) Spanish Research Council CSIC – Complutense University of Madrid UCM. Madrid, Spain (d.freire@igeo.ucm-csic.es, Rafael.fort@csic.es)
(2) CEI Campus Moncloa, UCM-UPM and CSIC, Madrid, Spain
(3) School of Geology. Complutense University of Madrid UCM. 28040 Madrid, Spain (mjvaras@geo.ucm.es)

*Corresponding author at: Instituto de Geociencias IGEO (CSIC, UCM), Calle José Antonio Novais, 12. 28040 Madrid. Tel.: +34 913944903. Fax: +34923219609. E-mail address: d.freire@igeo.ucm-csic.es

Abstract

Four types of granite widely exported and used in construction around the world were subjected to 280 accelerated freeze-thaw test cycles, conducted as stipulated in European standard UNE-EN 1237:2001 to ascertain their petrophysical response.

The techniques used to characterise the granite before and after freeze-thaw-induced microcracking included vacuum water absorption, ultrasonic P-wave pulse velocity and ultrasonic S-wave pulse velocity, mercury intrusion porosimetry and polarised optical and fluorescence microscopy to quantify the type of microcracks developing (inter-, intra- or transcrystalline) and identify the associated mineral phases: quartz, feldspar and biotite. The linear crack density (number of cracks per millimetre) was calculated based on the microscopic data collected. Young's modulus was likewise found before and after the freeze-thaw cycles.

The chief ice crystallisation mechanism involved in microcracking and hence deterioration was ice segregation. In all four granites, ultrasonic propagation velocities and strength parameters declined with the development of freeze-thaw-induced microcracking. More intercrystalline microcracks developed in the early cycles, while larger numbers of intracrystalline microcracks were found at the end of the test.

The results of this study can be applied to other granites with similar characteristics and whose microcracks are generated with same mechanisms of frost damage.

Upon conclusion of the cycles, Zarzalejo granite exhibited the largest number of microcracks, with a linear crack density of 3.9, as well as the highest rise in microcracking. Colmenar Viejo ended the freeze-thaw test with the fewest number of microcracks and a post-test linear crack density of 2.3, denoting greater freeze-thaw resistance. The smallest increase in the number of microcracks was found for Cadalso de los Vidrios granite.

The microscopic and microporosity findings reported in this paper revealed the existence of freeze-thaw test-induced microcracking which, while barely affecting mechanical stability (Young's modulus), did cause damage.

Keywords: granite, durability, weathering, freeze-thaw test, microcracks.

1 Introduction

Granite has been traditionally used as a building stone, in some countries because of quarry proximity to cities and in many others as a high quality import (Fort et al., 2013). Spain is the world's seventh largest producer of natural stone and the fourth largest exporter. Granite ships primarily to other European countries and North America for use in cities such as Vancouver, Paris, Cork, and Munich where temperatures dip below freezing over 30 times yearly, inducing frezze-thaw (FT) events. (Ruedrich and Siegesmund, 2007; Ruedrich et al., 2011).

Thousands of tonnes of these granites are exported annually for use as construction materials in prominent buildings. Some examples are the Cork International Airport terminal in Ireland, Place Romagné in France, and retail parks at Dortmund, Germany and Guangzhou, China. Hence, the need to meet high quality standards to ensure the optimal performance in all manner of situations (Siegesmund and Török, 2011).

The aim of the present study is to determine the quality of four widely used building granites to FT weathering, determined on the grounds of (P- and S-wave) ultrasonic pulse velocity, Young's modulus, linear crack density and porosity in several FT weathering stages. Damage was established by comparing the findings obtained with destructive and non-destructive techniques.

The objective of FT testing is to simulate natural weathering caused by ice at a faster pace in the laboratory (Halsey et al., 1998). This may induce rapid change in the physical and mechanical properties of these materials in humid open systems with widely fluctuating temperatures (Hudec, 1998; Iñigo et al., 2000; Gupta and Rau, 2001; Ehlen, 2002, Sanjurjo and Alves, 2006, Rivas-Brea et al., 2008; Hall et al., 2012; Jamshidi et al., 2013).

FT has a direct impact on landforms and building stone durability (Kieslinger, 1931). It limits durability not only in very cold regions, but also where freezing occurs during few days in temperate climates where temperatures occasionally drop to below freezing, particularly during

the night (Takarli et al., 2008). Where these cycles are frequent (Halsey et al., 1998), they generate fatigue in granite and cracks through which water can ingress.

When ice crystallisation pressure equals the tensile strength of the rock, further microcracks develop and the existing cracks deepen and widen, damaging the rock. Ice crystallisation and growth mechanisms in geomaterials have been the object of research for several decades (Hor and Morihiro, 1998; Scherer, 1999; Coussy and Fen-Chong, 2005). Several mechanisms exist to explain ice crystallisation-induced stress in wall cracks (Chen et al., 2004; Ingham, 2005; Ruedrich and Siegesmund, 2007).

The volumetric expansion of water during freezing: when water congeals its volume increases about 9 %, generating pressure on the walls of the cracks, which favours widening (Ozcelik et al., 2012). For cracking to be due only to the expansion associated with the water to ice phase change, the rock would have to be highly saturated. FT-induced natural damage occurs without such saturation. (Chen et al., 2004; Ruedrich and Siegesmund, 2007; Takarli et al., 2008).

Another mechanism is hydraulic pressure (Hor and Morihiro, 1998). The increase in volume attendant upon ice crystallisation confines the (liquid) water, which then places pressure on the walls of the cracks. This premise is based on the observation that ice crystallises as it moves deeper into the rock. Due to its increased volume, unfrozen water may ingress into the pore space. If insufficient expansion space is available near the ice front, stress is generated in the matrix. Other stress development models are based on osmotic pressure (Powers and Helmuth, 1953) and anomalous variations in ice density when it crystallises quickly.

Ice segregation (Tabor, 1929, 1930, Arakawa, 1965, Walder J and Hallet, 1985, Akagawa and Fukuda 1991, Hallet et al., 1991, Matsuoka and Murton, 2008) takes place in freezing or frozen microporous media. The unfrozen water held in microcracks and adsorbed onto the surfaces of mineral particles is forced by temperature gradient-induced suction through a porous medium

such as micro-cracked granite toward freezing sites where ice lenses, ribbons, needles, layers or strands grow (Murton et al., 2006). In other words, water that starts off widely dispersed in the porous rock segregates into discrete pieces of ice. Since water but not ice can flow through pores of this size, ice segregation is a major cause of cracking in moist, porous rocks (Matsuoka, 2001).

Frost damage may entail a combination of several mechanisms, although one or another generally predominates, depending upon conditions (Ingham, 2005). Water and temperature are the main weathering agents in FT ageing. As a rule, crystallisation begins in large surface cracks, for in smaller cracks ice crystallisation calls for colder temperatures. FT-induced decay in natural stone therefore depends largely on the existence of open cracks, the natural channels for water penetration into rock, and their post freezing development (Martínez-Martínez et al., 2013).

Ice crystallisation cracking in granite is not fully understood, since it depends on a number of factors (Hudec, 1998): the temperature range, the frequency of FT, the stress applied, water composition and moisture content, as well as internal factors such as rock mineralogical composition, texture, rock strength, characteristics of the existing pore microstructure and thermal conductivity of the constituents.

Preceded by elastic deformation in granite (Lajtai, 1998), in addition to existing crack closure and internal crack sliding, changes in the microcrack network affect the physical and mechanical properties of the rock and are responsible for the decay and anisotropy found in many granites (Fujii et al., 2007; Fort et al., 2011). Microcrack characteristics and the physical-mechanical properties of rocks are, then, essential considerations when assessing material durability (Matias and Alves, 2001; Sousa et al., 2005).

Mechanical strength in granites is related to a number of petrographic parameters, including: grain size (Tuğrul and Zarif, 1999; Akesson, 2001; Yilmaz et al., 2011), microstructural characteristics (Alm et al.,1985; Carvalho et al., 1997; Feng and Yu, 2000; Lindqvist et al., 2007; Vasconcelos et al., 2008; Nasseri and Mohanty, 2008), mineral composition (Miskovsky et al.,

2004), grain boundaries (Raisanen, 2004) and mineral shape and spatial arrangement (Akesson et al., 2003).

When destructive tests (such as static laboratory tests in heritage buildings) cannot be performed to determine the mechanical characteristics of the rock, the dynamic modulus must be found with non-destructive techniques such as ultrasonic testing (Brotons, 2014). As mechanical moduli are required to calculate the strain on new buildings generated by the live loads applied, pre- and post-FT Young's modulus values were calculated in this study.

Like other agents of rock decay such as wet/dry cycles, thermal shock and salt crystallisation, FT is regarded as a physical weathering agent (Jamshidi et al., 2013; Shalkowshi et al., 2009), weathering granite at a rate of several millimetres per thousand years (Chen, 2000). An understanding of the long-term durability of construction granite exposed to FT cycles is therefore in order. While decay function models have been developed to predict FT-induced deterioration of the mechanical properties of building stone (Bayram, 2012; Jamshidi et al., 2013; Mutlutürk et al., 2004), the respective equations are only valid for specific rocks.

Although FT testing has been standardised (UNE-EN 12371; TS 699, ASTM D5312; DIN 52104), the number of FT cycles applied and the physical property used to quantify FT action differ among standards. The effect of FT has therefore been studied from different perspectives for different types of rocks.

A sizeable number of studies have been conducted on freezing in building stones in recent decades. The number and duration of FT cycles and the temperature sequence and range applied in those studies varied widely. The concomitant inconsistencies in the findings (Cárdenes, 2014) must be borne in mind when comparing the results.

Ingham (2005) ran 50 cycles, for instance, compared to the 1 400 run by authors such as Ruedrich et al. (2011), Iñigo et al. (2000), García-del-Cura et al. (2008), Karaca et al. (2010), Jamshidi et al., (2013) applied 24-hour cycles, while in the Del Río et al. (2005) study cycle duration was 4 hours and in the Tan et al. (2011) survey, 8. The temperature ranges also varied: Ozcelik et al. (2012) established a low of -40 and a high of 180 °C, while in Wang et al. (2007) the interval ran from -7 to 14 °C.

Some authors measured FT-induced decay on the grounds of sample weight loss (Iñigo et al., 2000; Erguler, 2009) or variations in ultrasonic pulse velocity (Matsuoka, 1990; Takarli et al., 2008; Ruedrich, et al., 2011; Liu et al., 2012; Iñigo, et al., 2013). Others developed equations from which to infer microcrack distribution in granites (Sano et al., 1992; Takemura and Oda, 2006; Nara et al., 2011). Moreover, the intrinsic characteristics of the granite (mineralogy and texture) also impact the type of microcracking generated by FT (inter-, intra- or transcrystalline) and hence rock petrophysical properties and ultimately durability.

The matrix (Yavuz, 2011), pore size and pore size distribution are especially important factors in granite resistance to ice crystallisation. Many authors (Haynes and Sneck, 1972; Wolfenden and Winslow, 1991; Mallidi, 1996; Benavente et al., 2007; Martínez-Martínez et al., 2013,) contend, based on mercury intrusion porosimetry findings, that intra-pore crystallisation is favoured by slow capillary kinetics, while others (Oguchi and Yuasa, 2010) claim that these developments are driven by fast capillary kinetics.

The present study explored the physical and mechanical effects of FT testing on the quality of granite exported for use in construction. Microcracking favours soiling, lichen colonisation and in some cases, crystal detachment. An understanding of the performance of granite used in construction in climates prone to FT cycles will help choose the most suitable material for each place and use in both new construction and restoration.

2 Materials and methods

2.1 Rock samples

The four granites selected for the study, monzo-and leucogranites from Sierra del Guadarrama (Central System) in central Spain, have been traditionally used as building materials in Madrid and surroundings and are now used worldwide (Figures 1 and 2). Alpedrete (AL), Cadalso de los Vidrios (CA), Colmenar Viejo (CO) and Zarzalejo (ZA) granites (Fort et al., 2013) were studied to determine the effect of FT on their decay. These construction stones are found in plutons with different chemical compositions (Villaseca et al., 1998).

Alpedrete is a 350- km^2 monzogranite-granodiorite pluton with local porphyritic varieties located about 35 km north of the city of Madrid. The monzogranite has an equigranular texture with fine to medium crystals exhibiting small microgranular mafic enclaves.

Cadalso de los Vidrios is a biotitic leucogranite (Mejías et al., 2009) and monzogranite pluton; it lies about 65 km west of Madrid and covers 59 km^2. The monzogranite has an equigranular texture with medium to large crystals and local porphyry. The leucogranite, with fine crystals and a lower biotite content, was used for this study.

Colmenar Viejo is a monzogranite pluton located about 31 km north of the city of Madrid, characterized by very homogeneous greyish white rocks. Leucocratic, medium-to-coarse grain size, or even darker porphyritic varieties are occasionally present.

The Zarzalejo monzogranite pluton is located about 60 km northwest of the city of Madrid (García-del-Cura et. al., 2008). Two texturally different units can be distinguished: a grey unit and a porphyritic unit characterised by the presence of K-feldspar megacrystals in a medium-grained matrix. It exhibits microgranular mafic minerals with enclaves and xenoliths, usually sub-

rounded or ellipsoidal with a quartz dioritic composition and sometimes with a porphyritic texture (feldspar phenocrystals).

The samples were selected from outcrops close to old quarries where the granite was fresh and fracture-free. Seven cubic (5x5x5±0.5 cm) specimens of each of the four types were extracted at a low cutting speed (120 rpm) and low strain.

The petrological characteristics of the specimens tested and examples of buildings built with the respective granites are listed in Table 1 (modified from Fort et al., 2011).

2.2 Freeze–thaw test (FT Test)

FT testing was conducted as specified in European standard EN 12371: 2001 (with 280 instead of the stipulated maximum 240 cycles) in a FT chamber fitted with a control system to programme the FT cycles to an accuracy of ±1.0 °C. As described in the standard, the specimens were water-saturated at 20 °C and atmospheric pressure for 48±2 h. They were subsequently placed in an air-filled FT test chamber (dry conditions), where they were spaced no less than 10 mm apart and at least 20 mm from the side of the chamber. The temperature sequence in each 12-hour cycle was as follows: (i) the temperature was lowered from +20 to -8 °C in 2ºh (dry conditions); (ii) and then to -12 °C in 4 h (dry conditions); (iii) the chamber was automatically filled with water in 0.5 h until the specimens were completely submerged at temperatures of 5 to 20 ºC (wet conditions); (iv) the specimens remained submerged for 5 hours; and (v) the water in the chamber was emptied in 0.5 h.

The specimens were removed from the FT chamber after every 70 FT cycles up to a total of 280 and dried in a ventilated oven at 70 °C. They were then visually inspected and tested for water saturation to quantify frost action. One of the seven samples of each variety of granite tested was reserved for Hg porosimetry analysis and fractography during FT testing.

2.3 Effective porosity (Pe)

P_e furnishes information on fractures, microcracks and pores generated during the FT cycles. P_e was therefore measured prior to the FT test and after every 70 cycles, up to and including 280. The samples were consequently tested for this parameter using the natural stone method described in Spanish and European standard UNE-EN 1936. After oven-drying at 70 °C to a constant weight (variation in two consecutive weighings over 24 hours <0.1 %), they were stored in a desiccator for 30 min. Set in a vacuum chamber at 2 kPa for 2 h, they were slowly submerged in water and subsequently stored at atmospheric pressure for 24 h to ensure full saturation. The P_e values were calculated from equation (1)

$$P_e\ (\%) = [(Ws-Wd)/(Ws-Wh)] \times 100 \quad (1)$$

Where Wd is the weight of the dry specimens (after oven-drying at 70 ºC and desiccation for 30 min). Ws is the weight of 24-h water-saturated sample, and Wh is the weight of the sample submerged in water.

2.4 Bulk density (ρb)

ρb was measured using also the Spanish and European standard UNE-EN 1936, i.e., as the ratio between specimen mass and its bulk volume, from equation (2):

$$\rho b = [(Wd)/(Ws-Wh)] \times 1000\ (kg/m^3) \quad (2)$$

2.5 Ultrasonic pulse velocities (V_p and V_s)

The velocity of ultrasonic pulses travelling in a solid material depends on the density, porosity, mineralogy and elastic properties of the material (Wang et al., 2007; Yarbaş et al., 2007). Ultrasonic pulse velocity provides an accurate measure of the total damage to the material

(Takarli et al., 2008), while fracture measurement affords an indication of the nature of the damage, i.e., whether the loss in V_p and V_s were more likely to have been induced by the generation of new or the extension of existing microcracks.

V_p measurements were taken with CNS Electronics PUNDIT equipment (precision: ±0.1 μs) further to Spanish and European standard UNE-EN 14579 recommendations. The even and round (11.82 mm in diameter) 1 MHz transducers were affixed to the stone surface with Henkel Sichozell Kleister (a carboxymethyl cellulose) paste and water to enhance the transducer-stone contact and bond.

V_p was measured on each sample in the three orthogonal directions, using the mean of four consecutive measurements on each side of the cube as the accepted value. V_p was determined before the FT test and after 140 and 280 cycles.

V_s was taken with a Panametrics 5058 PR high voltage pulser-receiver connected to a Tektronix digital phosphorus oscilloscope (Model TDS 3012B).

Panametrics V151, 25.4-mm diameter, 0.5-MHz even and round transducers were affixed to the stone surface with a coupling gel consisting of 80 % sugar (primarily fructose and glucose) and 20 % water to enhance the transducer-stone contact and bond. The pulse repetition rate was 20 Hz and damping 200 Ohm.

V_s was measured on each sample in the three spatial directions, taking the mean for each specimen as the accepted value. V_p was determined before the FT test and after 280 cycles.

V_p and Vs were then used to compute Young's modulus (E_{dyn}) from the Darracott (1976) equation (Eq. (3)) and the V_p/V_s ratio.

$$E_{dyn}=\rho\,[3\,V_p^2-4V_s]/[(V_p/V_s)^2-1] \qquad (3)$$

where V_p is the longitudinal wave value (m/s); V_s, the transverse wave value (m/s); E_{dyn}, Young's modulus (Pa); and ρb, bulk density (kg/m^3).

The conversion from dynamic to static modules was based on Sousa's (2014) equation: $E_{st}=0.99E_{dyn} - 0.92$.

2.6 Mercury intrusion porosimetry (MIP)

MIP was conducted on a single prismatic specimen (12±2 mm in diameter and 20±2 mm high) cut from an upper corner of one of the cubic specimens. The analysis was run before and after FT testing on samples oven-dried to a constant weight at 70° C. A Micromeritics Autopore IV 9 520 porosimeter with a maximum pressure of 414 MPa (60 000 psi) was used to assess sample pore structure, including total porosity (pore diameter range: 0.001-400 μm), macro- and micro-porosity and pore size distribution. The cut-off between micro- and macro-porosity was set at a pore diameter of 5 μm (Russel, 1927; Rodríguez and Sebastián, 1994; Fort et al., 2011).

2.7 Fractography

A 30x20±3 mm thin section measuring, 30 μm thick was sectioned from one specimen of the AL, CA and ZA before FT testing and after each series of 70 cycles. Identical thin sections were cut from CO after 0, 70, 140 and 280 cycles. To ensure the thin section was removed from a surface of the specimen exposed to all FT cycles, successive thin sections were sawn off different sides of the specimen, parallel to and within 1 cm of the surface. Sawing was performed at low speed (120 rpm) and low strain so as not to generate artefacts (microcracks).

The thin sections were impregnated with fluorescence and characterised under an Olympus BX 51 polarized light microscope (PM) fitted with DP 12-coupled (6 V/2.5 Å) Olympus digital micrography and Olympus DP-Soft software (version 3.2). Cracks were characterised with the same equipment, as well as with the same set-up using an Olympus U-RF-T mercury lamp fluorescence microscope (FM).

PM and FM micrograph mosaics (Gale et al., 2010) were made from the thin sections to monitor microcrack development. Each mosaic comprised 40 micrographs of the same area, measuring approximately 4.5 cm^2. The cross-Nicols micrograph mosaics were used for mineral quantification, and the fluorescence mosaics to study cracks. One fragment of the FM mosaic was

laid over the same fragment of the PM mosaic and two squares were drawn on the resulting image, one measuring 1 cm^2 and the other 0.25 cm^2. The sides of these squares were drawn parallel to the two sides of the original FT-tested cubic specimen (Figure 3). Fracturing was quantified by counting the total number of microcracks that intersected with the sides of these squares, as well as the number that cut across quartz, feldspar and mica. A distinction was also drawn among microcracks found along the edge (intercrystalline) or inside (intracrystalline) crystals or that impacted more than one grain (transcrystalline). Intercrystalline microcracks were subdivided by the mineral interface involved: quartz/feldspar, quartz/biotite or feldspar/biotite. Lastly, the linear crack density (LCD) (Sousa et al., 2005) was calculated as the number of microcracks per millimetre. In other words, the LCD was found by counting the number of each type of fracture intersecting the boundary lines, with a total length of 50 mm, of the squares drawn on the mosaic.

3 Results

3.1 Bulk density (ρb), weight loss and effective porosity (Pe)

Initial ρb was similar in the four granites, ranging from 2 602 kg/m^3 in CA to 2 668 kg/m^3 in AL, and varied very little throughout the FT test: from 0.2 % in CA to 0.6 % in ZA. The initial P_e was low, at 0.7 % in CO to 1.7 % in ZA. The lowest post-FT cycle weight loss was recorded for CA and CO (0.6 %) and the highest for ZA (1.1 %). Porosity rose in all the granites after the FT cycles. Pre-and post-test weight, ρb and P_e of specimens are given in Table 2.

3.2 Cracks

Initial cracking was greatest in CA, followed in descending order by ZA, AL and CO. Crack rates rose with the FT cycles in all the materials studied (Table 3).

LCD rose steeply in CA after the first 70 cycles, but more moderately from then on through the end of the test. From the 70th to the 280th cycle, the pace was similar to the crack generation rate observed in CO, which held steady throughout the test. Total crack generation in CO was much more linear than in the other granites and post-280 cycle fracturing was also lowest in this variety.

The highest post-FT LCD was observed in ZA, where the fracture rate in the first 70 cycles was nearly as low as in AL and CO. The sharp rise was recorded after 140 and 210 cycles.

3.2.1 Relationship between type of fracturing and minerals involved

The same trend was observed in the four granites: similar numbers of existing microcracks were found, mostly in quartz and feldspar. No pre-cracking was detected in biotite.

Quartz exhibited the steepest rise in fracturing in the first 70 cycles, after which the slope of the curve tapered (Figure 4). Fracturing rose more sharply in feldspar in the final series, except in CA where the slope was steepest in the first 140 cycles. Very few microcracks developed in biotite. The earliest microcracks were observed in ZA after the first 70 cycles, whereas in the other granites no microcracking appeared until after 140 cycles or even after 210 cycles (CA).

3.2.2 Inter-, intra- and transcrystalline microcracks

Before FT testing, intercrystalline microcracks prevailed over the intracrystalline type. Intracrystalline microcracks grew in number as the FT test advanced. ZA had more intra- than intercrystalline microcracks after 70 cycles; CA had more intra-than intercrystalline microcracks after 140 and AL after 210, while CO only exhibited more intra- than intercrystalline microcracks after 280 cycles (Figure 5). In AL, the number of intracrystalline microcracks remained more or less constant through the first 140 cycles, growing after 210. With a sharper rise in the number of inter- than intracrystalline microcracks after 210 cycles, however, this was the only granite that had a larger number of intercrystalline than intracrystalline microcracks at the end of the FT test.

CA exhibited the lowest increase (30 %) in LCD for intercrystalline microcracks. The increase in intercrystalline microcracks was greatest in AL (180 %). The largest increase in intracrystalline microcracks, 505 %, was recorded for ZA, compared to 192 % for AL, where it was lowest (Table 4, Figure 5).

3.2.3 Relationship between fracture type (inter-, intra- trans-crystalline) and crystals

The proportion of inter-, intra- and transcrystalline microcracks in each granite varied with the number of FT cycles (Table 4). The fracture network was primarily intercrystalline in the earliest series. With each new series, feldspar developed more intracrystalline microcracks along its crystallographic planes of weakness. Biotite had the fewest intercrystalline microcracks.

The number of intercrystalline microcracks affecting quartz grew moderately in all four granites, by 12 % in ZA to a maximum of 61 % in AL. The intracrystalline microcracks in quartz rose more rapidly, by a minimum of 80 % in CO to a maximum of 625 % in AL. The number of intercrystalline microcracks increased more in feldspar than in quartz, from 35 % in CA to 225 % in AL. The number of intracrystalline microcracks after 280 cycles, in the four granites studied, is higher inside feldspar than inside quartz (Table 5). Figure 6 shows the pre- and post- FT testing microcracks for the four granites studied.

3.3 Ultrasonic pulse velocities (V_p and V_s)

Each granite had a characteristic initial V_p and V_s. The highest initial V_p was found in CO (5 051±349 m/s), followed by AL (4 620±163 m/s), CA (3 687±300m/s) and lastly ZA (3 219±204 m/s). V_p declined after the FT cycles in all four varieties of granite. The rate of decline in their post-280-cyle V_p was 2.8 % in CO, 2.9 % in CA, 3.8 % in AL and 5.2 % in ZA.

The highest initial V_s was found in AL (3 812±107 m/s), followed by CO (3 494±94 m/s), CA (2 596±110 m/s) and lastly ZA (2 2116±89 m/s). V_s declined after the FT cycles in all four

varieties of granite. The rate of decline in their post-280-cyle V_s was 2.7 % in CO, 2.8 % in AL, 3.0 % in CA and 4.7 % in ZA. The V_p/V_s ratio was similar for all granites: AL= 1.2; CA= 1.4; CO= 1.4 and ZA= 1.4.

E_{dyn} was initially highest in CO, followed by CA, AL and lastly ZA. E_{dyn} declined after the FT cycles in all four varieties of granite. The specimens exhibited different rates of decline in their post-280-cyle V_s values: 5.8 % in CO, 6.0 % in CA, 10.2 % in ZA and 21.9% in AL. Table 6 gives E_{dyn} and E_{st} for the four types of granites tested.

3.4 Mercury intrusion porosimetry (MIP)

According to the Hg intrusion findings, the granite with the highest initial porosity was ZA followed by CA, CO and AL in descending order. Porosity as determined by Hg intrusion rose during FT testing in all the granites except CO (Table 7).

The initial microporosity followed essentially the same pattern as porosity in the four granites, i.e., the greatest microporosity was observed in ZA and CA, followed by AL and CO. Microporosity also rose in all four materials after the FT cycles. The pore size distribution graphs (Figure 7) showed a rise in microporosity in all the granites: by 7.6 % in ZA, 15.1 % in CA, 16.3 % in AL and 25.4 % in CO.

4 Discussion

Other FT studies conducted on granite under conditions similar to those described here (Del Río et al., 2005; García-del-Cura et al., 2008; Karaca et al., 2010; Liu et al., 2012; Jamshidi et al., 2013), in which fewer than 70 cycles were run, could not determine the changes actually impacting these materials. Ruedrich et al., 2011 noted that clear evidence of damage was only observable after over 50 FT cycles, although the FT testing conditions, i.e., temperature, cooling rate and water pressure inside the microcracks, affect microcrack generation and damage

substantially. In nearly 100 % saturated, closed system rocks, volumetric expansion is the ice crystallisation mechanism that governs microcracking. These were not the conditions prevailing in the present tests nor in granites used as ashlars or façade cladding, however. Such rocks may be affected by ice segregation, another mechanism that induces microcracking and hence deterioration. The suction temperature induced by the FT chamber generated a freezing gradient in the granite samples, with ice concentrating on the surface of the specimens. The water inside the granites migrated through the microcracks to the surface, where the ice grew, inducing surface microcracks. Murton et al., (2006) contended that for ice segregation to prompt microcracking in highly porous chalk, the temperature must hover around 0 °C, whereas Walder and Hallet (1985) claimed that in low porosity rock such as granite cracking is most intense when the temperature ranges from -4 to -15 °C at a rate of 0.1 to 0.5 °C/h. At the cooling rate and temperatures proposed in Spanish and European standard UNE-EN 1237:2001 and used here, i.e., 14 °C/h in the temperature range +20 to -8 °C and 1 °C/h between -8 and -12 °C, ice crystallised on the specimen surface. This may have occurred when the outside temperature was below zero and the temperature inside the specimens was above zero, enabling the interstitial water to flow across the microcracks to the surface.

The petrophysical and mechanical properties of studied in the four granites varied to some degree after the FT cycles. CO exhibited the lowest LCD, MIP, P_e and the highest $V_{p,}V_s$ and E_{st}, denoting a higher resistance to FT. Conversely, ZA showed the least resistant post-FT test petrophysical and mechanical characteristics.

The smallest rise in P_e, ρb, LCD and weight loss was observed in CA. These factors also increased minimally in CO, which had the lowest decline in V_p. The smallest growth in microporosity was recorded for ZA, the granite with the steepest rises in P_e, ρb, weight loss and LCD and the sharpest decline in V_p. As CA has a smaller crystal size than the other granites, it exhibited the highest initial and final intercrystalline LCD. ZA, the granite with the largest crystal size due to the presence of large feldspar crystals, developed the highest number of intracrystalline microcracks.

Through the first 70 FT cycles, microcrack development was similar in the four granites. The intercrystalline type initially accounted for 54 to 64 % and after the 70th cycle, from 56 to 63 % of all the cracking detected, except in ZA, which after the 70th cycle had 43 % intercrystalline microcracks. Following the first 70 cycles, all the granites developed more intracrystalline microcracks, albeit in different proportions. At the end of the test (280 cycles), intracrystalline microcracking predominated in all except AL. This result was consistent with prior granite weathering studies (Sousa et al., 2005), which reported intracrystalline microcracks to be the most frequent form of cracking.

Takemura et al. (2003) and Takemura and Oda (2004), who also distinguished between microcracks in quartz and feldspar (as well as in terms of grain boundaries), found that microcrack generation differed in these minerals. The present quantification of microcracks on PM and FM micrographs showed that intracrystalline fracturing was greater in feldspar than in quartz. Sousa et al. (2005) reported that over half of the cracks detected in ornamental granites were intracrystalline and located on feldspar crystals. These authors noted that microcracks often appeared in the cleavage direction, a finding observed as well in the scanning electron microscope images published by Manchao et al. (2010).

The FT test induced greater inward confinement stress in the cracks developing along both the edges of the crystals and their planes of weakness. Nonetheless, no microcracking was found in the areas between quartz and biotite, inasmuch as the laminar texture of biotite affords it sufficient flexibility and ductility to reduce cracking, particularly in the cleavage direction. In other types of accelerated ageing tests (salt crystallisation) conducted on AL and ZA (López-Arce, 2010), biotite was observed to be more heavily impacted by surface microcracks. However, according to the present FM findings for thin sections taken at a depth of 1 cm, biotite was the mineral that developed the fewest fractures inside the granite.

Scant transcrystalline microcrack proliferation was observed in all four granites. Transcrystalline microcracking appeared in different forms and at different stages of the FT test. Transcrystalline

microcracks, which were larger than the inter- and intra-crystalline varieties, were the result of interconnections, normally when an intercrystalline fracture spread in the cleavage direction. Microscopic quantification of the fractures showed that ZA exhibited the largest number of transcrystalline fractures, weakening inter-crystalline boundaries and favouring grain detachment. This finding is consistent with the fact that weight loss was greatest in ZA.

These fractures were the reason that the P_e was greater than could be detected with MIP, which detect microcracks <400 μm. MIP nonetheless revealed a rise in microporosity in all the specimens. Iñigo et al. (2000) ruled out the use of MIP because the extremely high pressures required to fill the narrowest pores induce microcracking. The consistency among the findings for P_e, porosity and microporosity observed with MIP in the present study before and after FT testing (Table 5) was an indication that MIP is suitable for this type of analyses. In fact, it is primarily used to determine microporosity, which rose in all the granites studied. Microporosity development was greatest in ZA, the most porous granite, and lowest in CO, the least porous granite studied.

Tuğrul and Zarif (1999) and Yilmaz et al. (2011) reported an inverse relationship between K-feldspar crystal size and mechanical strength in granites. Larger crystals have longer edges, favouring the propagation of intercrystalline microcracks, while the cleavage typical of potassium feldspars, which act as the weakest planes, facilitates intragranular microcracking (Eberhardt et al., 1999; Chen et al., 1999; Wong et al., 2006). In the present study, the K-feldspar content in ZA, its larger crystal size and larger number of initial microcracks contributed to its lower E_{st}. Nonetheless, CO, with larger K-feldspar crystals than AL and CA, had a higher pre-and post-FT test E_{st}. That effect was the result of its lower pre- and post-trial micro- and effective porosities and its higher V_p than the other three granites. The PM and FM findings for each granite explain their E_{st} values. Despite the similarity in the number and size of potassium feldspar crystals in ZA and CO, the former exhibited the highest and the latter the lowest LCD. Microcracks generate strain under stress. Benmeddour et al. (2012) reported a linear correlation between E_{st} and porosity. The decline in E_{st} with exposure to FT cycles denotes a reduction in rock elasticity.

However, E_{st} remained high after FT testing in all the specimens studied here was an indication that the granite underwent no severe internal damage, inasmuch as the cracks generated did not affect the inside of the samples.

The V_p/V_s ratios found for the granites studied resembled the values reported by Liu et al. (2012) for a granite subjected to 30 FT cycles. V_p/V_s remained essentially unchanged after FT testing in the present research because the deterioration induced in the four granites was not critical.

Microcrack proliferation has adverse effects on granite quality, soiling building stones and favouring both lichen colonisation (De la Torre et al., 2010) and water circulation. Such cracking ultimately induces disaggregation, crumbling and detachment of the constituent crystals, with the concomitant loss of surface volume.

5 Conclusions

Parameters monitored in this study complement one another and are needed to quantify and assess granite microcracking during FT cycles. V_p and V_s are sensitive to the presence of microcracks but less sensitive to their number and type. This technique, which delivers valuable information for determining durability, affords the advantages of portability, ease of use and speed. P_e furnished information on the largest microcracks, while data on micropore development was gleaned from MIP.

While the four granites studied were mineralogically similar and the FT test conditions applied and ice crystallisation mechanisms were the same in all four, their clearly distinct textures explained their differential decay when exposed to FT cycles. The pre- and post-test findings provided clear evidence of the quality and durability of these four building granites and their resistance to FT events, attributable to their high density, low porosity and high V_p and V_s.

Nonetheless, the FT test had an adverse effect on the petrophysical and mechanical properties of all the granites, in which microcracking was the main sign of the decay induced by the test.

Resistance to FT was greatest in CO due to its texture and especially to its lesser initial cracking, while ZA was the least resistant to FT testing. This lesser durability was attributable to the greater initial cracking and high feldspar crystal content in ZA.

Ice crystallises in microcracks existing in the granite, whose intrinsic properties determine microcrack development. Intracrystalline microcracking, especially along cleavage planes or areas of crystalline weakness, was greatest in feldspar and lowest in biotite. LCD rose most in the granite with the largest crystal size (ZA) and least in the granite with the smallest crystal size (CA). At the end of the test, ZA had the highest P_e, MIP, weight loss and LCD and the lowest V_p, V_s and E_{st} while the lowest decay was observed in CO. The granites where intracrystalline microcracks appeared earliest were the ones with the highest rate of decay.

The minor decline in E_{st} recorded for the four granites studied was an indication of their high mechanical resistance to FT, which would explain their centuries long endurance in good condition in heritage buildings, despite the microcracks observed in PM and FM analysis.

FT test conditions such as maximum and minimum temperatures, the minimum number of cycles and petrographic monitoring of weathering should be standardised for each type of rock. The number of FT cycles applied and the physical property used to quantify FT action differ among standards.

Acknowledgements

This study was funded by the Community of Madrid under the GEOMATERIALS project (S2013/MIT-2914). The authors are members of the Complutense University of Madrid's Research Group: "Alteración y Conservación de los Materiales Pétreos del Patrimonio" (ref. 921349). The authors wish to thank the Geological and Mining Institute of Spain for conducting

the FT chamber tests. The petrophysical assessments were run at the IGEO Petrophysical Laboratory, affiliated with the Moncloa Campus of International Excellence (UCM-UPM) Heritage Laboratory Network (RedLabPat). The assistance, input and support provided by laboratory technicians Andrés Lira, Cristina Cedazo and Blanca Gallardo are gratefully acknowledged.

Manuscript edited by Margaret Clark, professional translator and English language science editor.

References

Alm, O., Jaktlund, L.L., Kou, S., 1985. The influence of microcrack density on the elastic and fracture mechanical properties of Stripa granite. Physics of the Earth and Planetary Interiors. 40 (3), 161–179.

Akagawa, S., Fukuda, M., 1991, Frost heave mechanism in welded tuff: Permafrost and Periglacial Processes 2, 301–309.

Akesson, U., Lindqvist, J.E., Gö ransson, M., Stigh, J., 2001. Relationship between texture and mechanical properties of granites, central Sweden, by use of image- analyzing techniques. Bull Eng Geol Environ .60, 277–84.

Akesson, U., Stigh, J., Lindqvist, J.E., Gö ransson, M., 2003. The influence of foliation on the fragility of granitic rocks, image analysis and quantitative microscopy. Eng Geol. 68, 275–88.

Arakawa, K., 1965. Theoretical studies of ice segregation in soil. Journal of Glaciology. 6 (44), 255–260.

ASTM D5312 / D5312M – 12. 2013. Standard Test Method for Evaluation of Durability of Rock for Erosion Control under Freezing and Thawing Conditions.

Bayram, F., 2012. Predicting mechanical strength loss of natural stones after freeze–thaw in cold regions. Cold Regions Science and Technology. 83–84, 98–102.

Benavente, D., Cueto, N., Martínez-Martínez, J., García Del Cura, M.A., Cañaveras, J.C., 2007. The influence of petrophysical properties on the salt weathering of porous building rocks. Environmental Geology. 52, 197–206. Doi: 10.1007/s00254–006–0475–y.

Benmeddour, F., Villain, G., Abraham, O., Choinska, M., 2012. Development of an ultrasonic experimental device to characterise concrete for structural repair. Construction and Building Materials. 37, 934–942.

Brotóns Torres, V., Tomás Jover, R., Ivorra Chorro, S., 2014. Estudio de la influencia de la temperatura en las propiedades físicas y mecánicas de la calcarenita de San Julián. Rehabend 2014, congreso latinoamericano. Patología de la construcción, tecnología de la rehabilitación y gestión del Patrimonio. 469–476. ISBN: 978–84-616–8863–0.

Cárdenes, V., Mateos F.J., Fernández-Lorenzo, S., 2014. Analysis of the correlations between freeze–thaw and salt crystallization tests. Environ Earth Sci. 71, 1123–1134 DOI 10.1007/s12665–013–2516–7.

Carvalho, F., Chen C.N.; Labuz, J., 1997. Measurements of effective elastic modulus and microcrack density. Int. J. RockMech. &Min. Sci. 34, 3–4, Paper No. 043

Chen Y, Nishiyama T, Kusuda H, Kita H, Sato T., 1999. Correlation between microcrack distribution patterns and granitic rock splitting planes. Int J Rock Mech Min. 36, 535–41.

Chen, T.C., 2000. Study on mechanisms of rock deterioration and rock slope failures in cold regions. PhD dissertation, Kitami Institute of Technology.

Chen, T.C., Yeung, M.R., Mori, N., 2004. Effect of water saturation on deterioration of welded tuff due to freeze-thaw action. Cold regions Science and Technology 38, 127–136.

Coussy, O., Fen-Chong, T., 2005. Mecanique Crystallization, pore relaxation and micro-cryosuction in cohesive porous materials. Comptes Rendus Mécanique, 333 (6), 507–512.

Darracott, B.W., Orr, C.M., 1976. Geophysics and rock engineering. Symp. On Exploration for Rock Engineering. Johannesburg. 1, 159–164. Cape Town/Rotterdam: Balkema.

De la Torre, R., Sancho, L., Horneck, G., de los Ríos, A., Wierzchos, J., Olsson-Francis, K., Cockell, C., Rettberg, P., Berger, T., De Vera, J.P., Ott, S., Martinez-Frías, J., González-Melendi, P., Mercedes-Lucas, M, Reina, M., Pintado, A., Demets, R., 2010. Survival of lichens and bacteria exposed to outer space conditions – Results of the Lithopanspermia experiments. Icarus 208, 735–748.

Del Río, L.M., López, F., Esteban F.J., Tejado, JJ., González, Mº.I., Ramos, A., San Emeterio, J.L., 2005 Ultrasonic study of Alteration Processes in Granites Caused by Freezing and Thawing. IEEE Ultrasonic Symposium.

DIN 52 104 Testing of natural stone; freeze-thaw cyclic test. (Deutsche norm)

Eberhardt, E., Stimpson, B., Stead, D., 1999. Effects of grain size on the initiation and propagation of thresholds of stress induced brittle fractures. Rock Mech Rock Eng. 32, 81–9.

EN 12371. Natural Stone tests methods: determination of frost resistance. Bruxelles: European Committee for Standardization; 1966.

Ehlen, J., 2002. Some effects of weathering on joints in granitic rocks. Catena 49, 91–109.

Eissa E.A., Kazi, A., 1988. Relation between static and dynamic Young's Moduli of rocks. Int J Rock Mech Min Sci. 25(6), 479–482. Doi: 10.1016/0148–9062(88)90987–4.

Erguler, Z., Shakoor, A., 2009. Relative contribution of various climatic processes in disintegration of clay-bearing rocks. Engineering Geology. 108, 36–42.

Feng X.Q., Yu S.W., 2000. Estimate of effective elastic moduli with microcrack interaction effects. Theoretical and Applied Fracture Mechanics. 34, 225–233.

Fort, R. Varas, M.J., Álvarez de Buergo, M., Freire-Lista, D.M., 2011. Determination of anisotropy to enhance the durability of natural Stone. Journal of geophysics and engineering. 8, 1–13. S132–S144 doi:10.1088/1742-2132/8/3/S13.

Fort, R., Álvarez de Buergo, M., Pérez-Monserrat, E.M., Gómez-Heras, M., Varas-Muriel, M.J., Freire-Lista, D.M., 2013. Evolution in the use of natural building stone in Madrid, Spain. Quarterly Journal of Engineering Geology and Hydrogeology. 46, 421–429. Doi: 10.1144/qjegh2012–041.

Fujii, Y. Takemura, T., Takahashi, M., Lin, W., 2007. Surface features of uniaxial tensile fractures and their relation to rock anisotropy in Inada granite. International Journal of Rock Mechanics & mining scienes. 44, 98–107.

Gale, J., Landerb, R., Reeda, R., Laubach, S., 2010. Modeling fracture porosity evolution in dolostone Journal of Structural Geology. 32, 1201–1211.

García-del-Cura, M.A., Benavente, D., Bernabéu, A., Martínez-Martínez, J., 2008. The effect of surface finishes on outdoor granite and limestone pavers. Materiales de Construcción. 58, 289–290, ISSN: 0465–2746 eISSN: 1988–3226.

Gupta, A.S and Rao, K.S., 2001 weathering indices and their applicability for crystalline rocks. Bulletin of Engineering Geology and the Environment. 60, 201–221. Doi: 10.1007/s100640100113.

Hall, K., Thorn, C., Sumner, P., 2012. On the persistence of 'weathering' Geomorphology. 149–150, 1–10.

Hallet, B, Walder, J.S., Stubbs, C.W., 1991. Weathering by segregation ice growth in microcracks at sustained subzero temperatures: Verification from an experimental study using acoustic emissions. Permafrost and Periglacial Processes. 2, 283–300.

Halsey, D.P., Mitchell, D.J., Dews, S.J., 1998. Influence of climatically induced cycles in physical weathering. Quarterly Journal of Engineering Geology and Hydrogeology. 31, 359–367.

Haynes, J.M., Sneck, T., 1972. Pore properties in the evaluation of materials. National Bureau of Standards Special Publication. 361 (1), 669–675.

Hor, M., Morihiro, H., 1998. Micromechanical analysis on deterioration due to freezing and thawing in porous brittle materials. International Journal of Enginering Sciences. 36 (4), 511–522.

Hudec, P.P., 1998. Rock properties and physical processes of rapid weathering and deterioration. 8th International Congress of IAEG. 1, 335–341.

Ingham, J.P., 2005. Predicting the frost resistance of building stone. Quarterly Journal of Engineering Geology and Hydrogeology. 38, 387–399.

Iñigo, A.C., Vicente, M.A., Rives, V., 2000. Weathering and decay of granitic rocks: its relation to their pore network. Mechanics of Materials. 32, 555–560.

Iñigo, A.C., García-Talegón, J., Vicente-Tavera, S., Martín-González, S., Casado-Marín, S., Vargas-Muñoz, M., Pérez-Rodríguez, J.L., 2013. Colour and ultrasound propagation speed changes by different ageing of freezing/thawing and cooling/heating in granitic materials. Cold Regions Science and Technology. 85, 71–78.

Jamshidi, A. Reza-Nikudel, M., Nikudel, Khamehchiyan, M., 2013. Predicting the long-term durability of building stones against freeze–thaw using a decay function model. Cold Regions Science and Technology. 92, 29–36.

Karaca, Z., Deliormanli, A., Elçi, H., Pamukcu, C., 2010. Effect of freeze–thaw process on the abrasion loss value of stones. International Journal of Rock Mechanics & Mining Sciences. 47, 1207–1211.

Kieslinger, A.,1931 Das Volumen des Eises. Geologie und Bauwesen. 2, 199–207.

King M.S., 1983. Static and dynamic elastic properties of rocks from the Canadian Shield. Int J Rock Mech Min Sci. 20 (5), 237–241. Doi: 10.1016/0148-9062(83)90004-9.

Lam dos Santos, J., Amaral, P., Diogo, A., Rosa, L., 2013 Comparison of Young Moduli of Engineered Stones using Different Test Methods Key Engineering Materials. 548, 220–230.

Lajtai, E.Z., 1998. Microscopic fracture Processes in a Granite. Rock Mechanic and rock engineering. 31 (4), 237–250.

Lindqvist J.E, Akesson, U, Malaga, K., 2007. Microstructure and functional properties of rock materials. Mater Charact. 58, 1183–8.

Liu, H., Niu, F.J., Xu, Z.Y., Lin, Z.J., Xu, J., 2012. Acoustic experimental study of two types of rock from the Tibetan Plateau under the condition of freeze-thaw cycles. Sciences in Cold and Arid Regions. 4(1), 0021–0027.

López-Arce, P., Varas-Muriel, M.J., Fernández-Revuelta, B., Álvarez de Buergo, M., Fort, R., Pérez-Soba, C., 2010. Artificial weathering of Spanish granites subjected to salt crystallization tests: Surface roughness quantification. Catena. 83, 170–185.

Manchao, H., Wen, N., Liqiang, H., Lijing, L., 2010. Microcrack analysis of Sanya grantite fragments from rockburst tests. Mining Science and Technology. 20, 0238–0243.

Mallidi, S.R., 1996. Application of mercury intrusion porosimetry on clay bricks to assess freeze-thaw durability Construction and Building Materials. 10, 461–465.

Matias, J.M.S., Alves, C.A.S., 2001. Decay patterns of granite stones in Braga monuments (NW Portugal) Historical Constructions, 363–371.

Martínez-Martínez, J., Benavente, D., Gómez-Heras, M., Marco-Castaño, L., García-del-Cura M.A., 2013. Non-linear decay of building stones during freeze–thaw weathering processes. Construction and Building Materials. 38, 443–454.

Matsuoka, N., 1990. Mechanisms of rock breakdown by frost action: an experimental approach. Cold Regions Science and Technology. 17, 253–270.

Matsuoka, N., 2001. Microgelivation versus macrogelivation: towards bridging the gap between laboratory and field frost weathering. Permafrost and Periglacial Processes. 12, 299–313.

Matsuoka, N., Murton, J., 2008: Frost Weathering: Recent Advances and Future Directions. Permafrost and Periglacial Processes. 19, 195–210.

Mejías, M., Renard, P., Glenz, D., 2009. Hydraulic testing of low-permeability formations A case study in the granite of Cadalso de los Vidrios, Spain. Engineering Geology. 107, 88–97.

Miskovsky K, Taborda Duarte M, Kou S.Q., Lindqvist P.A., 2004. Influence of the mineralogical composition and textural properties on the quality of coarse aggregates. J Mater Eng Perform. 13, 144–50.

Murton J.B., Peterson, R. Ozouf. J.C., 2006. Bedrock Fracture by Ice Segregation in Cold Regions. Science. 314, 1127–1129.

Mutlutürk, M., Altindag, R., Türk. G., 2004. A decay function model for the integrity loss of rock when subjected to recurrent cycles of freezing–thawing andheating–cooling. International Journal of Rock Mechanics & Mining Sciences. 41, 237–244.

Nara, Y., Kato, H., Yoneda, T., Kaneko, K., 2011. Determination of three-dimensional microcrack distribution and principal axes for granite using a polyhedral specimen International Journal of Rock Mechanics & Mining Sciences. 48, 316–335.

Nasseri, M.H.B., Mohanty, B., 2008. Fracture toughness anisotropy in granitic rocks. Int J Rock Mech Min Sci. 45, 167–93.

Oguchi, C.T., Yuasa, H., 2010. Simultaneous wetting/drying, freeze/ thaw and salt crystallization experiments of three types of Oya tuff. Geological Society, London, Special Publications. 59–72.

Ozcelik, Y., Careddu, N., Yilmazkaya. E., 2012. The effects of freeze–thaw cycles on the gloss values of polished stone surfaces. Cold Regions Science and Technology. 82, 49–55.

Powers, T.C., Helmuth, R.A., 1953. Theory of volume changes in hardened Portland-cement paste during freezing, Highway research Board. 32, 285–297.

Prikryl R., 2001. Some microstructural aspects of strength variations in rocks. Int J Rock Mech Min. 38, 671–82.

Raisanen M., 2004. Relationships between texture and mechanical properties of hybrid rocks from the Jaala-Iitti complex, southeastern Finland. Eng Geol. 74, 197–211.

Rivas-Brea, T., Prieto Lamas, B., Silva Hermo, B., 2008. Ensayos de alteración artificial aplicados a rocas graníticas. Materiales de Construcción. 58, 289-290, 179–189.

Rodríguez, C., Sebastián, E., 1994. Técnicas de análisis del sistema poroso de materiales pétreos ornamentales: usos y limitaciones. Ingeniería Civil. 96, 130–142.

Ruedrich, J., Siegesmund, S., 2007. Salt and ice crystallisation in porous sandstones. Environmental Geology. 52, 225–249.

Ruedrich, J., Kircher, D., Siegesmund, S., 2011. Physical weathering of building stones induced by freeze-thaw action: a laboratory long-term study. Environmental Earth Sciences. 63, 1573–1586.

Russel, S.A., 1927. Stone preservation committee report (Appendix I). H.M. Stationary Office, London.

Sanjurjo, J., Alves, C.A.S., 2006. Degradación de rocas graníticas empleadas como material de construcción en edificios históricos de A Coruña (NW España) Cadernos Laboratorio Xeolóxico de Laxe. 31, 11–28.

Sano, O., Kudo Y, Mizuta Y., 1992. Experimental determination of elastic constants of Oshima granite, Barre granite, and Chelmsford granite. Journal of Geophysical Research. 97, 3367–79. Doi: 10.1029/91JB02934.

Scherer, G.W., 1999. Crystallization in pores Cement and Concrete. Cement and Concrete Research. 29, 1347–1358.

Shalkowshi, A., Kodama, Y., Nakano. S., 2009. The assessment of weathering stages in granites using an EC/pH meter. Geomorpholgy. 105, 253–260.

Siegesmund S., Török A., 2011. Building stones. In: Siegesmund, S., Snethlage, R. (Eds) Stone in architecture—properties, durability, 4th edn. Springer, Berlin. 11–96.

Sousa, L.M.O. Suárez del Río, Luis M., Calleja, L., Ruiz de Argandoña, V.G. Rodríguez A., 2005. Influence of microfractures and porosity on the physico-mechanical properties and weathering of ornamental granites. Engineering Geology. 77, 153–168.

Sousa, L.M.O., 2014. Petrophysical properties and durability of granites employed as building stone: a comprehensive evaluation. Bull Eng Geol Environ. 73, 569–588.

Tabor, S., 1929. Frost heaving. Journal of Geology. 37, 428–461.

Tabor, S., 1930. The mechanics of frost heaving. Journal of Geology. 38, 303–317.

Takarli, M., Prince, W., Siddique, R., 2008. Damage in granite under heating/cooling cycles and water freeze–thaw condition. International Journal of Rock Mechanics & mining Sciences. 45, 1164–1175.

Takemura, T., Golshani, A., Oda, M., Suzuk, K., 2003. Preferred orientations of open microcracks in granite and their relation with anisotropic elasticity International Journal of Rock Mechanics & Mining Sciences. 40, 443–454.

Takemura, T., Oda, M., 2004. Stereology-based fabric analysis of microcracks in damaged granite. Tectonophysics. 387, 131–150.

Takemura T, Oda M., 2006. Changes in crack density and wave velocity in association with crack growth in triaxial tests of Inada granite. International Journal of the Japanesee Committee for Rocks Mechanics Geophysical Research. 2 (1), 13–16.

Tan, X., Chen, W., Yang, J., Cao, J., 2011. Laboratory investigations on the mechanical properties degradation of granite under freeze–thaw cycles. Cold Regions Science and Technology. 68, 130–138.

TSE 699, 1987. Methods of Testing for natural building stones. Institute of Turkish Standards, Turk Standartları Enstitusu (TSE). p. 82.

Tuğrul, A., Zarif I.H., 1999 Correlation of mineralogical and textural characteristics with engineering properties of selected granitic rocks from Turkey. Eng Geol. 51, 303–17.

UNE-EN 12371:2011 Natural stone test methods–Determination of frost resistance.

UNE-EN 14579:2005 Natural stone test methods–Determination of sound speed propagation.

UNE-EN 1936:2007 Natural stone test methods–Determination of real density and apparent density and of total and open porosity.

Vanheerden, W.L., 1987. General relations between static and dynamic moduli of rocks. Int J Rock Mech Min Sci. 24(6), 381–385.

Vasconcelos, G., Lourenço, P.B., Alves, C.A.S., Pamplona, J., 2008. Experimental character ization of the tensile behaviour of granites. Int J Rock Mech Min. 45, 268–77.

Villaseca, C., Barbero, L., Rogers, G., 1998. Crustal origin of Hercynian peraluminous granitic batholiths of Central Spain: petrological, geochemical and isotopic (Sr, Nd) constraints. Lithos. 43, 55–79.

Wang, D., Ma, W., Niu Y-N., Chang, X-X., Wen Z., 2007. Effects of cyclic freezing and thawing on mechanical properties of Qinghai–Tibet clay. Cold Regions Science and Technology. 48, 34–43.

Walder J, Hallet, B., 1985. A theoretical model of the fracture of rock during freezing. Geological Society of America Bulletin. 96, 336–346.

Wolfenden, A. Winslow, D., 1991. Predicting the durability of paving bricks. Journal of Testing and Evaluation. 19 (l), 29–33.

Wong, R.H.C., Lin, P., Tang, C.A., 2006. Experimental and numerical study on splitting failure of brittle solids containing single pore under uniaxial compression. Mech Mater. 38, 142–59.

Yarbaş, N., Kalkan, E., Akbulut, S., 2007. Modification of the geotechnical properties, as influenced by freeze–thaw, of granular soils with waste additives. Cold Regions Science and Technology. 48, 44–54.

Yavuz, H, 2011. Effect of freeze–thaw and thermal shock weathering on the physical and mechanical properties of an andesite stone. Bulletin of Engineering Geology and the Environment. 70, 187–192.

Yilmaz Günes, N., Mete Goktan, R., Kibici, Y., 2011. Relations between some quantitative petrographic characteristics and mechanical strength properties of granitic building stones. International Journal of Rock Mechanics & Mining Sciences. 48, 506–513.

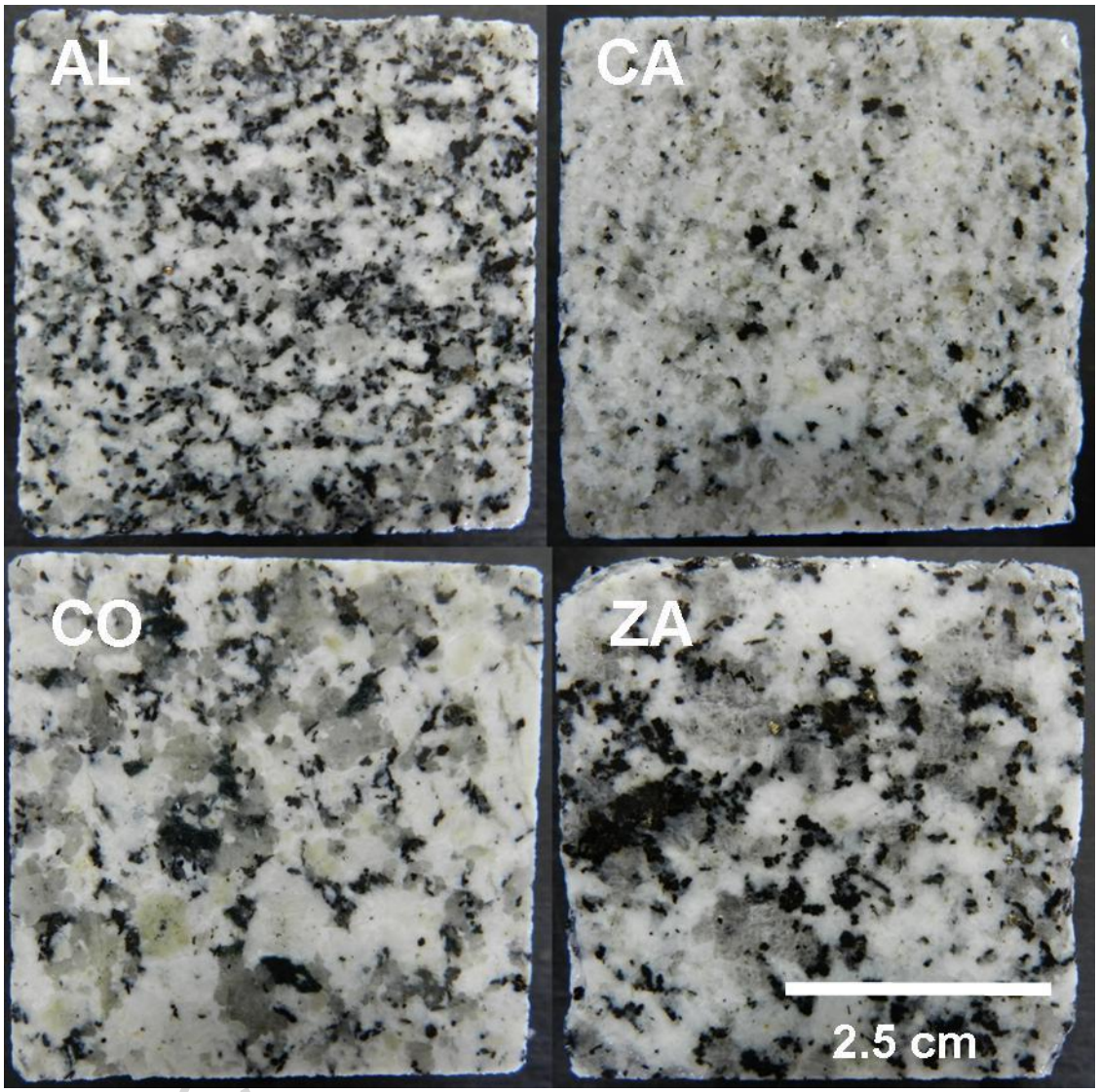

Fig. 1. Post-FT test surface (25 cm^2) of four granite specimens; AL: Alpedrete granite; CA: Cadalso de los Vidrios granite; CO: Colmenar Viejo granite; ZA: Zarzalejo granite

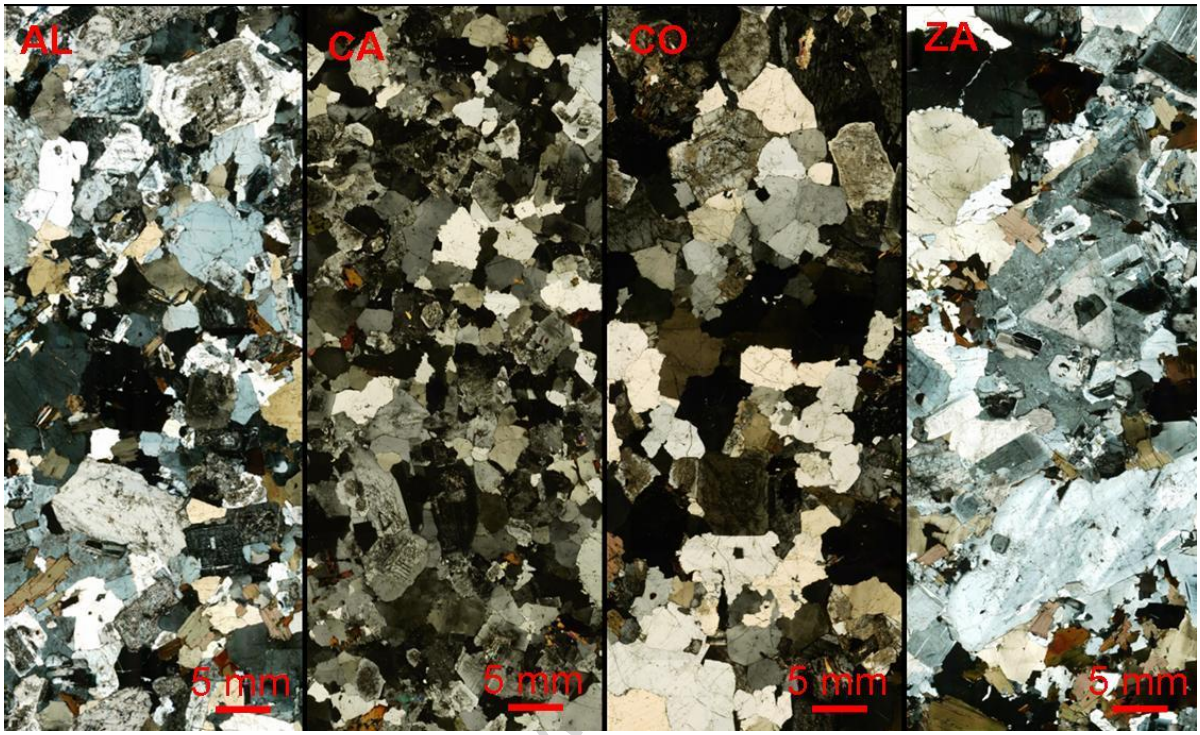

Fig. 2. Polarised light petrographic micrographs of the four granites studied; AL: Alpedrete granite; CA: Cadalso de los Vidrios granite; CO: Colmenar Viejo granite; ZA: Zarzalejo granite

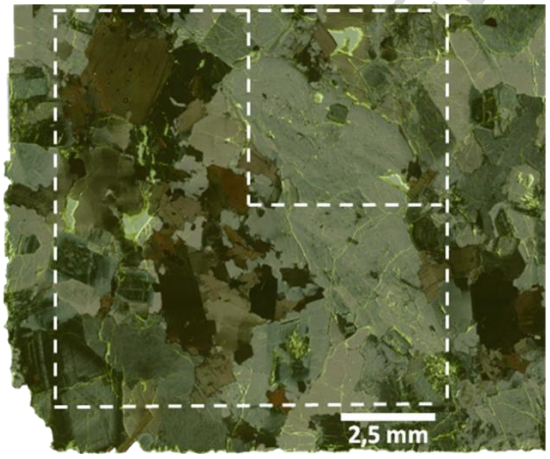

Fig. 3. Thin section of ZA specimen: fragment of an FM micrograph mosaic overlaid on the same fragment of a PM micrograph mosaic, showing the sides of the two squares (50 mm, linear) on which LCD was measured

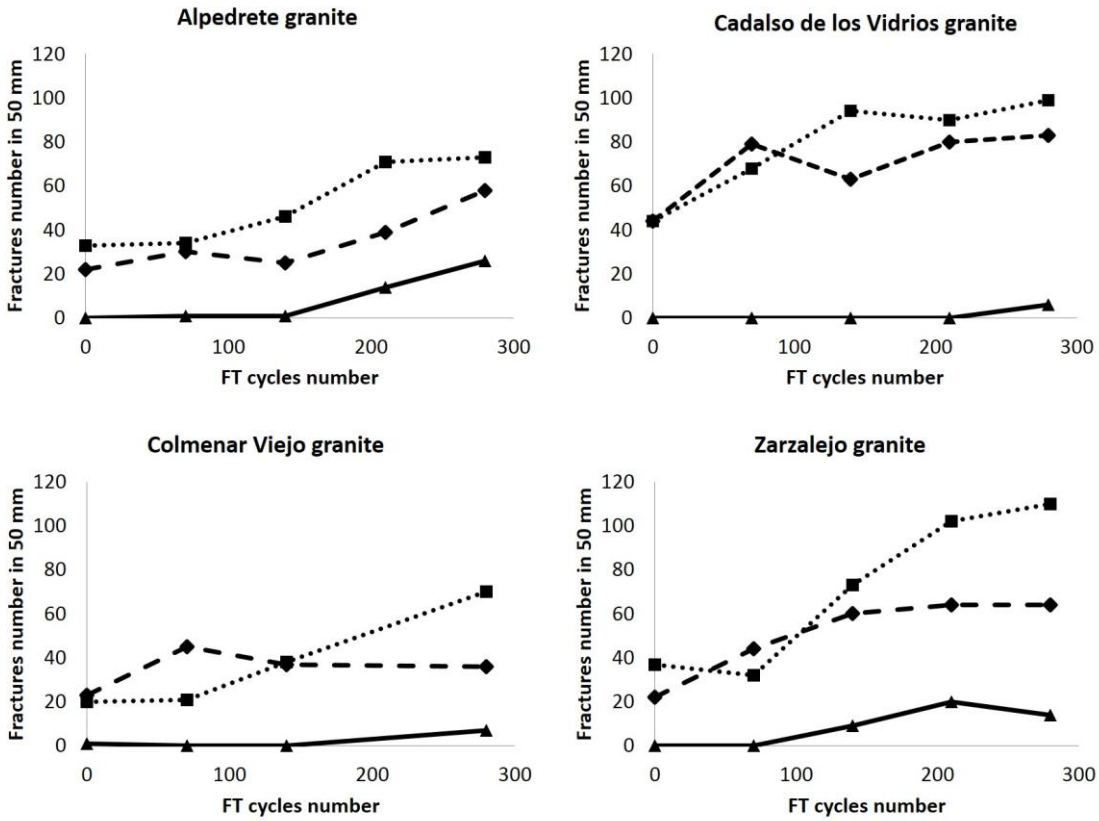

Fig. 4. Number of fractures in 50 mm (linear) of the four granites exposed to FT test, by mineral: quartz (rhombi), feldspar (squares) and biotite (triangles)

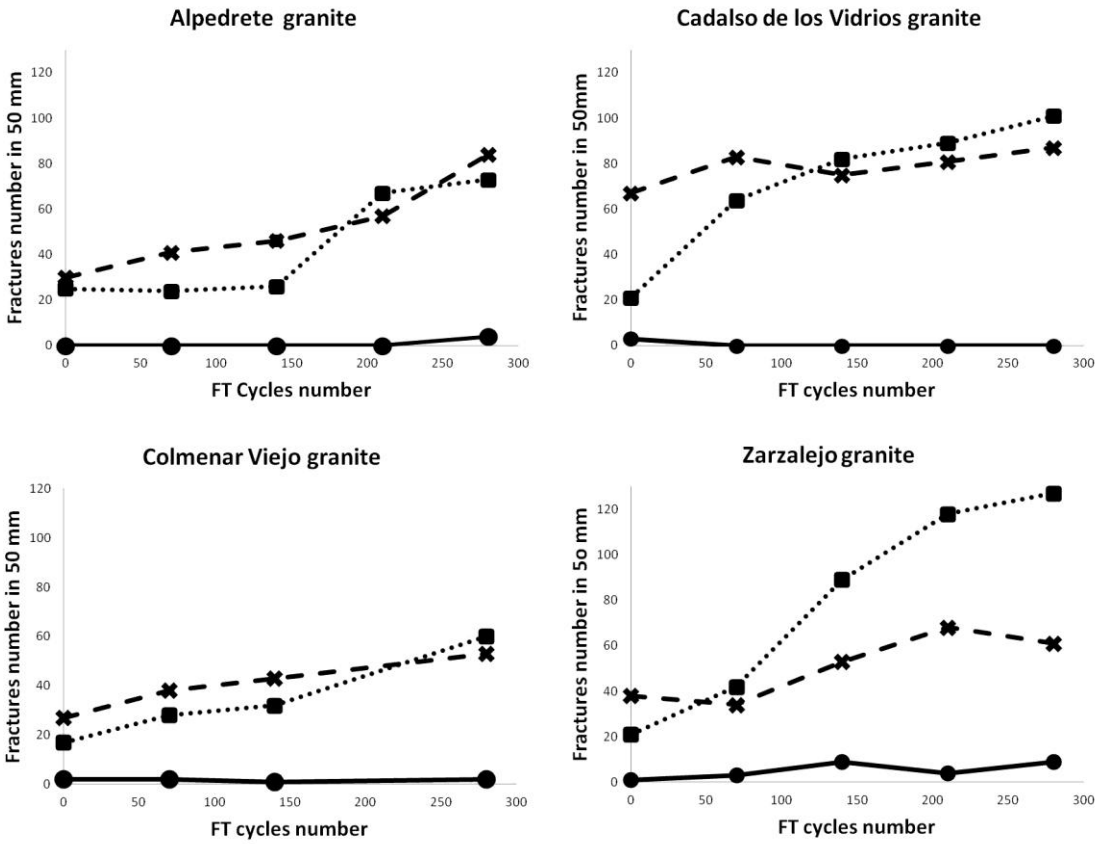

Fig. 5 Number of microcrack developing vs. number of FT test cycles by type of microcrack and granite studied (Inter-crystalline microcracks: x-marks; intra-crystalline microcracks, squares; trans-crystalline microcracks: circles)

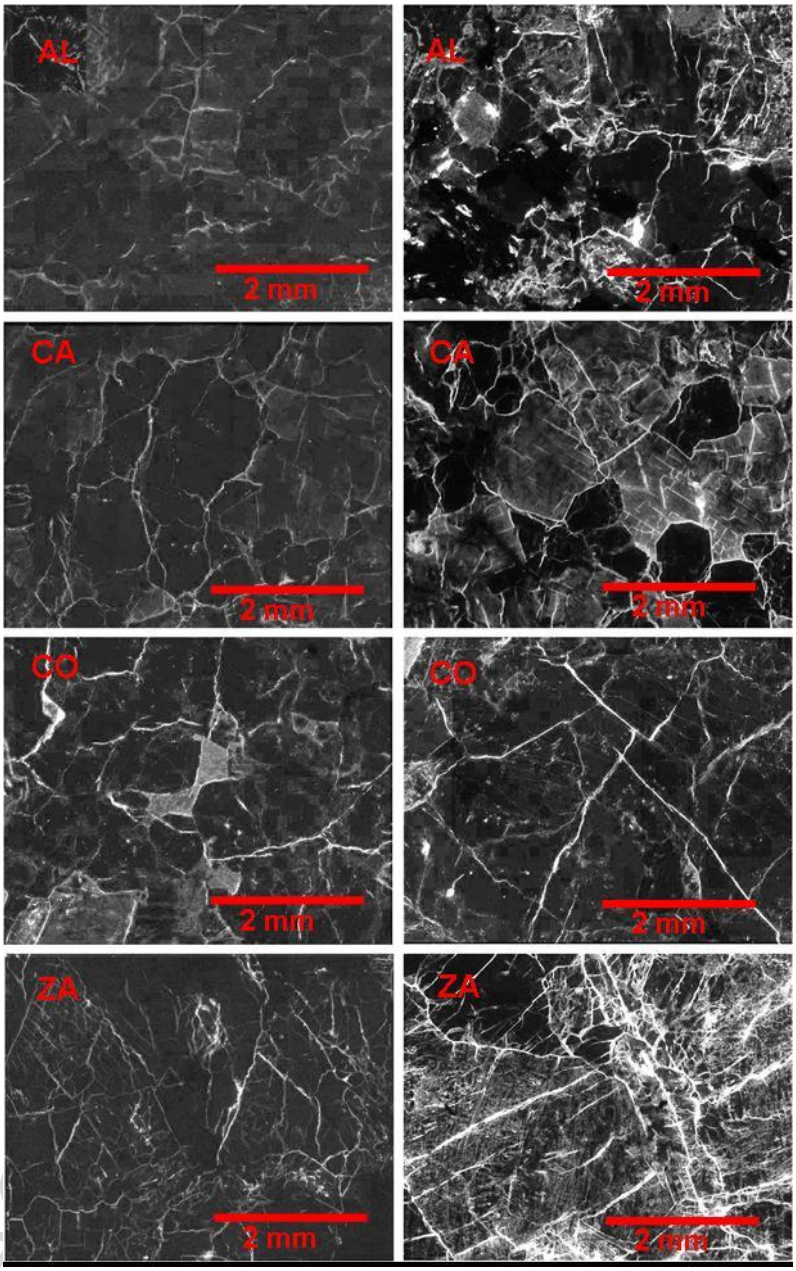

Fig. 6. Fluorescence microscope images of granite samples (AL: Alpedrete granite, CA: Cadalso de los Vidrios granite, CO: Colmenar Viejo granite, ZA: Zarzalejo granite); left: before FT testing; right: after 280 FT cycles

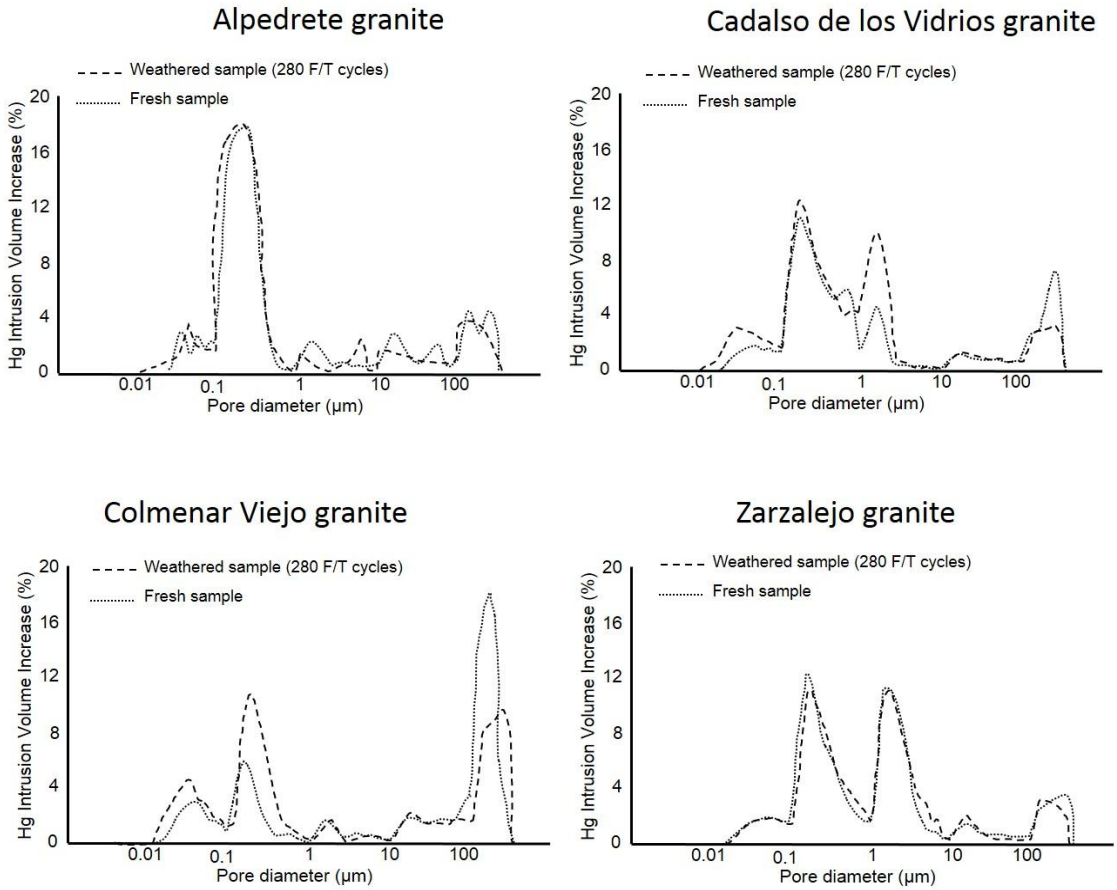

Fig. 7. Pore size distribution (PSD) graphs for four granites exposed to FT testing; dotted line: specimen pore size distribution of the specimens prior to FT testing; dashes: pore size distribution after 280 FT cycles

Table 1. Four granites studied: type, petrographic description, accessory minerals and heritage buildings on which they are found

Granite Name	Type	Textural properties and mineralogical composition	Accessory minerals	Buildings
Alpedrete (AL)	Monzogranite	Medium-grained, hypidiomorphic, equigranular. Quartz (2–3 mm and 40–50 % vol.), plagioclase (1–3 mm and 20–25% vol.), K-feldspar (microcline; 2–4 mm and 10–15% vol.) and biotite (1– 2 mm and 10–15% vol.)	Ilmenite, cordierite, apatite, zircon and monazite.	Nuestra Señora de la Asunción Church-fortress at Alpedrete, Royal Palace and Alcalá Gate at Madrid.
Cadalso de los Vidrios (CA)	Leucogranite	Fine-medium-grained, hypidiomorphic, equigranular. Quartz (1–3 mm and 50–55 % vol.), plagioclase (1–3 mm and 20–25 % vol.), K-feldspar (1–4 mm and 20–25 % vol.) and biotite (0.5–2 mm and 3–5 % vol.)	Zircon, apatite, monazite, sphene, ilmenite, allanite and some opaque minerals.	Casa de los Austria, Asunción Church and Villena Palace at Cadalso de los Vidrios. Cork International airport. Vieux Port, Marseille.
Colmener Viejo (CO)	Monzogranite	Medium-coarse-grained, heterogranular. Quartz (2–7 mm and 30–40 % vol.), plagioclase (2–7 mm and 20–25 % vol.), k-feldspar (3–6 mm and 20–25 % vol.) and biotite (1–5 mm and 7– 10 % vol.)	Cordierite, muscovite, apatite, zircon and opaque minerals.	Roman road and Asunción Basilica at Colmenar Viejo.
Zarzalejo (ZA)	Monzogranite	Coarse-grained, hypidiomorphic, heterogranular. Quartz (2–7 mm and 30–40 % vol.), plagioclase (3– 9 mm and 15–20 % vol.), K-feldspar (4–9 mm and 25–30 % vol.) and biotite (2–6 mm and 10–15 % vol.)	Apatite, zircon, opaque minerals and monazite.	San Pedro el Apóstol Church, Royal Monastery of San Lorenzo de El Escorial, Encarnación and Descalzas Reales Monasteries at Madrid. Royal Palace at Madrid y Moncloa Palace (restoration)

Table 2. Pre- and post-FT test values of effective porosity and bulk density in four granite varieties

Granite	Cycle 0		Cycle 280		Δ Weight (%)	Δ Effective porosity (%)	Δ Bulk density (%)
	Effective Porosity (%)	Bulk density (kg/m^3)	Effective porosity (%)	Bulk density (kg/m^3)			
AL	0.8±0.08	2668±18	0.9±0.22	2 660±7	-0.9	10.5	-0.3
CA	1.2±0.20	2602±16	1.3±0.18	2 596±45	-0.6	6.0	-0.2
CO	0.7±0.12	2629±13	0.8±0.16	2 620±5	-0.6	7.1	-0.3
ZA	1.7±0.06	2657±15	1.9±0.01	2 640±26	-1.1	11.6	-0.6

Table 3 Linear crack density (LCD) for four granite varieties, before FT testing and after 70, 140, 210 and 280 cycles

Linear crack density by number of FT cycles (cracks per mm)						
Granite	**0**	**70**	**140**	**210**	**280**	**Δ 0 to 280 (%)**
AL	1.1	1.3	1.44	2.48	3.22	193
CA	1.82	2.94	3.14	3.4	3.76	107
CO	0.92	1.36	1.52	--	2.3	150
ZA	1.2	1.58	3.02	3.8	3.94	228

Table 4: Inter- and intracrystalline linear crack density (LCD) after FT testing for four granites.

Linear crack density (cracks per mm) by FT cycle fracture type												
Granite	**0 cycles**		**70 cycles**		**140 cycles**		**210 cycles**		**280 cycles**		**Δ 0 to 280 (%) Inter**	**Δ 0 to 280 (%) Intra**
	Inter	**Intra**	**Inter**	**Intra**	**Inter**	**Intra**	**Inter**	**Intra**	**Inter**	**Intra**		
AL	0.6	0.5	0.82	0.48	0.92	0.52	1.14	1.34	1.68	1.46	180	192
CA	1.34	0.42	1.66	1.28	1.5	1.64	1.62	1.78	1.74	2.02	30	381
CO	0.54	0.34	0.76	0.56	0.86	0.64	-	-	1.06	1.2	96	253
ZA	0.76	0.42	0.68	0.84	1.06	1.78	1.36	2.36	1.22	2.54	61	505

Table 5. Number of intra- and intergranular microcracks (affecting a line of 50 mm) in quartz and feldspar for four granites

Granite	**Microcracks type**	**Quartz microcracks**					
		0 cycles	**70 cycles**	**140 cycles**	**210 cycles**	**280 cycles**	**Δ (%)**
AL	**Inter**	18	20	18	21	29	61
	Intra	4	10	7	18	29	625
CA	**Inter**	33	46	28	37	37	12
	Intra	11	33	35	43	46	318
CO	**Inter**	13	26	20	-	18	38
	Intra	10	19	17	-	18	80
ZA	**Inter**	16	20	21	27	22	37
	Intra	6	24	39	37	42	600
Granite	**Microcracks type**	**Feldspar microcracks**					
		0 cycles	**70 cycles**	**140 cycles**	**210 cycles**	**280 cycles**	**Δ (%)**
AL	**Inter**	12	20	27	29	39	225
	Intra	21	14	19	42	34	62
CA	**Inter**	34	37	47	44	46	35

	Intra	10	31	47	46	53	430
CO	**Inter**	13	12	23	-	31	138
	Intra	7	9	15	-	39	457
ZA	**Inter**	22	14	28	31	31	41
	Intra	15	18	45	71	79	426

Table 6. Pre- and post- FT test dynamic Young's moduli, E_{dyn} (Darracott, 1976) (left) and static Young's moduli, E_{dyn} (Sousa, 2014) (right) for four granites

E_{dyn} Darracott, 1976			**E_{st} Sousa, 2014**	
***Edyn*=ρ [3 Vp2-4Vs]/[(Vp/Vs)2-1]**			**E_{st}=0.99 E_{dyn} -0.92**	
Granite	**Initial E_{dyn} (MPa)**	**Final E_{dyn} (MPa)**	**Initial E_{st} (MPa)**	**Final E_{st} (MPa)**
AL	33612	26238	33275	25975
CA	35377	33243	35023	32910
CO	66838	62931	66169	62301
ZA	27155	24393	26882	24148

Table 7. Porosity and microporosity as determined by Hg intrusion for four granites: pre- and post-accelerated ageing

Granite	**Porosity (%)**		**Microporosity (%)**		**Δ (%) Porosity**	**Δ (%) Micro-porosity**
	0 cycles	**280 cycles**	**0 cycles**	**280 cycles**		
AL	0.44	0.5	0.31	0.36	13.6	16.3
CA	0.95	0.96	0.67	0.77	1.1	15.1
CO	0.59	0.47	0.17	0.22	-20	25.4
ZA	1.4	1.48	1.06	1.14	5.5	7.6

Highlights

It’s required to have a correct unification according to the FT test standards under more number of cycles.
The analysis of microcracks with MF permits study their characteristics and quality.
The granites with the highest initial fracture developed after FT test greater number of fractures.
In granites, feldspars are mineral that generate the greatest number of fractures under FT test.
The different texture in each granites determined differential decay.